Journal of Coastal Research	9	2	434–447	Fort Lauderdale, Florida	Spring 1993

Response of Louisiana Coastal Environments to a Cold Front Passage

Christopher C. Moeller†, Oscar K. Huh‡, Harry H. Roberts‡, Liam E. Gumley* and W. Paul Menzel††

†Cooperative Institute for Meteorological Satellite Studies
225 W. Dayton Street
Madison, WI 53706, U.S.A.

‡Louisiana State University
Coastal Studies Institute
Howe-Russell Geosciences Complex
Baton Rouge, LA 70803, U.S.A.

*Research and Data Systems Corporation
7855 Walker Drive, Suite 460
Greenbelt, MD 20770, U.S.A.

††NOAA/NESDIS Advanced Satellite Products Project
1225 W. Dayton Street
Madison, WI 53706, U.S.A.

ABSTRACT

MOELLER, C.C.; HUH, O.K.; ROBERTS, H.H.; GUMLEY, L.E., and MENZEL, W.P., 1993. Response of Louisiana coastal environments to a cold front passage. *Journal of Coastal Research*, 9(2), 434–447. Fort Lauderdale (Florida), ISSN 0749-0208.

The effect of a cold front passage on suspended sediment concentrations, water temperatures, and coastal circulation off Louisiana is examined via remote sensing with the Multispectral Atmospheric Mapping Sensor (MAMS). This 12 channel visible-infrared scanning spectrometer is flown on NASA's ER-2 aircraft, collecting 100 m resolution data over a 37 km swath from an altitude of 20 km. Time series charts of water temperature and suspended sediment content record the rapid (days) response of these shallow coastal waters to the cold front system of March 30–April 1, 1989. The river discharge sediment plumes stream down wind from the coast, remaining as coherent discrete water masses for up to 100 km. Detectable temperature gradients evolve rapidly in the estuarine waters in response to changing atmospheric conditions, with lowest temperatures developing in shallowest regions. Water level setup and setdown created by surface winds and barometric pressure strongly affect the exchange of river, estuarine and Gulf water. Behavior of the turbid river and estuarine discharge plumes is important as they serve as the source for new sediment deposits along the coastline. The utility of time series from high resolution, multispectral imagery in coastal environmental research, resource management, and pollution control is clear from this short term, multimission coverage.

ADDITIONAL INDEX WORDS: *Geomorphology, estuaries, sea surface temperature, suspended sediment.*

INTRODUCTION

The role of cold front weather systems in coastal geomorphology has only in recent years become a topic of research. These weather systems have been extensively studied from meteorological and climatological points of view because they affect most of the developed world. However, their importance as agents of change in coastal environments is just being recognized. Cold fronts, because of their higher frequency of occurrence, larger area of coverage, and persistent sequence of wind shifts from repeated directions of approach, are thought to be affecting the coastal environment more on a cumulative basis than the occasional tropical storm. ROBERTS *et al.* (1987) have outlined responses of various portions of the Louisiana coastline to passing cold fronts. These include deposition and erosion at different parts of the coastline, suspended sediment transport, and water level setup and wave action which alternately cause inland marsh inundation and drainage. KEMP (1986) has suggested that wave action associated with winter storms transports fluid mud in coastal waters, promoting progradation of shoreface where fluid mud is present. Understanding the mechanisms of coastal change and their response to cold front systems is necessary in order to develop effective coastal management programs.

The Multispectral Atmospheric Mapping Sensor (MAMS) has been used to study the impact of a cold front which passed through the Louisiana coastal zone on March 30–31, 1989. MAMS data was collected in daytime cloud-free conditions during the pre-frontal phase on March 30 and in day two of the post-frontal phase on April 1. MAMS has been used in previous work along the Louisiana coastline (MOELLER *et al.*, 1989)

92022 received 9 March 1992; accepted in revision 4 August 1992.

Table 1. *MAMS spectral channels.*

Channel	Bandwidth (@ 50% response)
1[a]	0.42–0.45 μm
2	0.45–0.52
3	0.52–0.60
4	0.57–0.67
5	0.60–0.73
6	0.65–0.83
7	0.72–0.99
8	0.83–1.05
9	3.47–3.86
10	3.47–3.86
11	10.55–12.24
12	12.32–12.71

[a] Not available when 10 bit infrared data are collected

and is well suited to monitor the coastal environment because of its 100 meter resolution in 12 spectral channels. The 12 visible/infrared channels are shown in Table 1. MAMS flies onboard NASA's ER-2 high altitude aircraft, scanning a 37 km swath from an altitude of 20 km. Calibration of infrared channels is accomplished by viewing two onboard blackbodies of known temperature during each scan. Visible calibration is accomplished by laboratory procedure. For detailed information on the MAMS spectrometer, see JEDLOVEC *et al.* (1989).

LOUISIANA COAST

Figure 1 shows the Louisiana coastal region and study sites. Three regions, the Atchafalaya Bay, the Chenier Plain, and the Chandeleur Islands (barrier islands) are circled in Figure 1 as locations of primary interest to the study. The Atchafalaya Bay is a region of new delta growth. Clays, silts and fine sands are transported by the Atchafalaya River, a distributary of the Mississippi River, into the Atchafalaya Bay. The sands and coarse silts are deposited in a series of delta lobes surrounding the mouths of both the Atchafalaya River and the Wax Lake Outlet. Clays and fine silts largely remain in suspension and are transported seaward and along shore by discharge inertia, and westward by prevailing coastal currents. These fine grained sediments drift westward in a sediment plume or mud stream where they are either deposited on the shoreface or settle out on the seafloor fronting the Chenier Plain. New deposits of fluid mud and mud congealed to clay have been found along the Chenier Plain (HUH *et al.*, 1991). Since 1987, a stretch over 14 km long along the Chenier Plain has been prograding seaward at the rate of some 60 meters per year (HUH *et al.*, 1991). This land is being formed when storm wave and surge action throw fluid mud onshore. The fluid mud supply has two possible immediate sources:

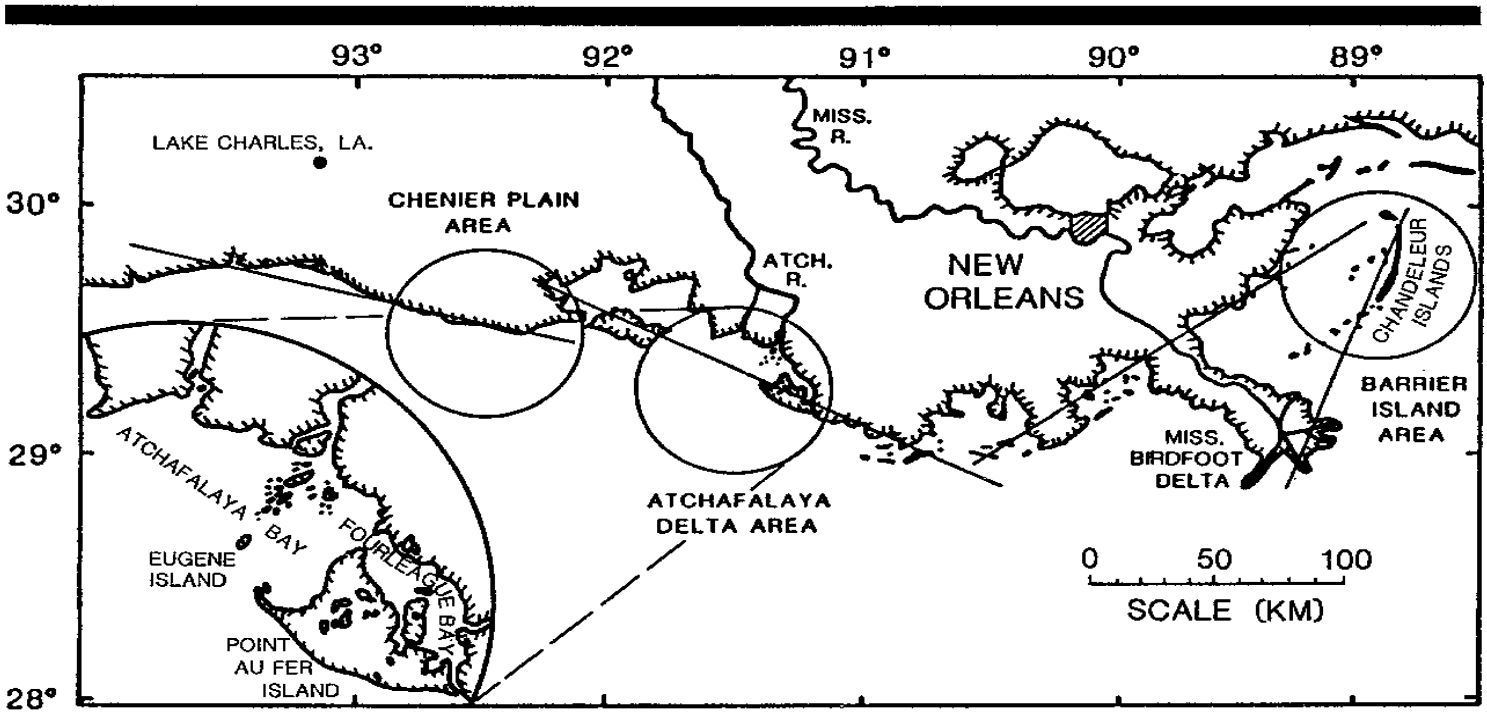

Figure 1. Louisiana coastal region with MAMS flight tracks (long thin lines) and primary areas of interest (circled) in the study. The Atchafalaya Delta area is expanded in the lower left hand corner for detail.

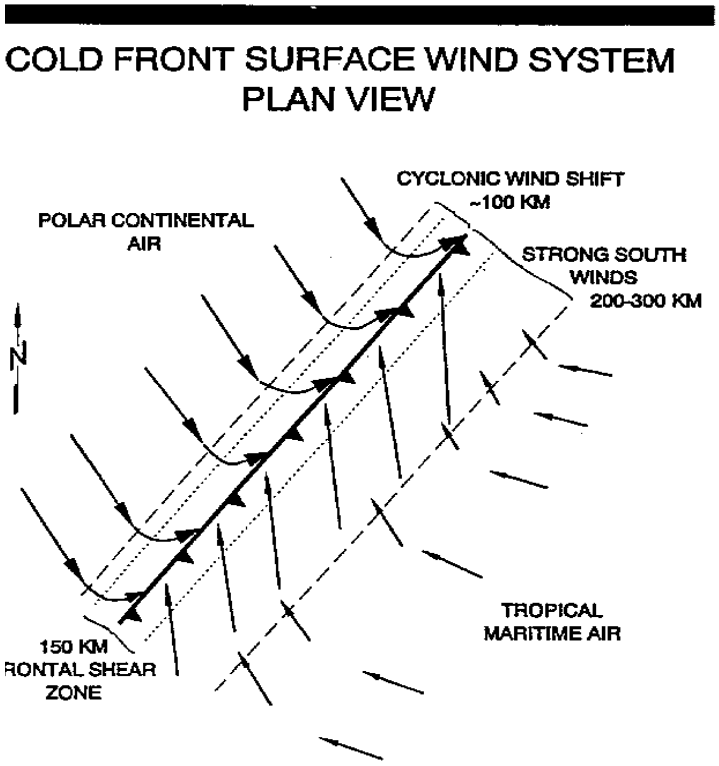

igure 2. Winds of the cold front system (from ROBERTS *et* ., 1987).

.) previously deposited seafloor material (from ıe Atchafalaya Bay sediment plume) resuspend- l by storm wave action, and (2) mud freshly recipitated from the coast-hugging Atchafalaya ud stream. The extent and flow path of this ud-stream/sediment-plume is of primary im- ortance for understanding land growth (and loss) atterns along the Chenier Plain. It will be shown ter than the behaviour of the sediment plume om Atchafalaya Bay is affected differently by ıe different phases of a cold front passage. In ntrast, the Chandeleur Islands, a series of sandy arrier islands off eastern Louisiana, are sediment arved and eroding. Storm waves and surge cause osion and destruction of this barrier island/ each/dune geomorphic complex. Images showing sponses of discharge plumes from the Missis- ppi River birdfoot delta channels are used to rther illustrate the response of coastal waters the cold front system.

THE COLD FRONT MODEL

About 30 to 40 cold fronts pass through the ouisiana coastline each year between the months October and April. These cold fronts have a atially and temporally ordered system of changes surface wind speed, wind direction, barometric pressure, temperature, and humidity (ROBERTS *et al.*, 1987). Figure 2 summarizes the wind system of a passing cold front. The cold front consists of three basic phases: (1) the pre-frontal phase (ahead of the front) in which southerly component winds dominate and warm, humid atmospheric conditions exist with generally falling barometric pressure, (2) the frontal passage phase, with strong and variable winds and a characteristic sharp shift of wind direction from a southerly to a westerly component, and (3) the post-frontal or cold air outbreak phase (behind the front) in which winds become northerly and air temperature and humidity decrease significantly with rising barometric pressure. Along the Louisiana coastline, pre-frontal phase southerly winds drive saline water into coastal bays and marshes. Onshore wave action created by the southerly winds erodes sediment starved sandy portions of the coastline while depositing sediment along muddy regions of the coastline (such as portions of the Chenier Plain). After the cold front passes, winds shift to a northerly direction driving down water levels in coastal areas and reducing onshore wave action. The dry cold air behind the front rapidly dries newly formed deposits on the shoreface, thus expediting the sediment consolidation of the coastal progradation process (HUH *et al.*, 1991). Water levels continue to drop, promoting marsh drainage and discharge of bay waters onto the continental shelf of the Gulf of Mexico. Coastal water temperatures also respond, cooling most rapidly in shallow regions.

Figure 2 represents an idealized model, a plan view of the surface wind fields associated with a cold front as it advances from NW to SE. The natural variability of cold fronts through the season includes: their orientation, direction of propagation (west to east, or north to south), strength (characterized by pressure gradient force, temperature and humidity characteristics), and speed of propagation. These factors will determine in large part the kind and amount of impact that a cold front passage will have on a coastal region. While the ordered pattern of change in a cold front passage is similar from case to case, there is much individual variability.

DATA PRODUCTS

Atmospheric Correction of Visible Radiances

MAMS visible and near infrared radiances are corrected for atmospheric effects to isolate the radiance upwelling from the water. Using mod-

elling studies, GORDON (1978), and GORDON *et al.*, (1983), developed a single scattering atmospheric correction method. The total radiance, L, arriving at the sensor is expressed as the sum of molecular scattering (L_r), aerosol scattering (L_a), sun glint (L_g), and the water leaving radiance (L_w) diffusely transmitted by the atmosphere.

$$L = L_r + L_a + L_g + tL_w$$

The diffuse transmittance t is used rather than the direct transmittance to account for the sensor receiving photons from regions adjacent to the field of view under examination.

Molecular scattered path radiance L_r and aerosol scattered path radiance L_a are expressed as the sum of photons scattered in the atmosphere directly into the sensor, and photons scattered in the atmosphere and then reflected back by the surface into the sensor. Expressions for molecular scattering optical depth and ozone optical depth (absorption) are given by GUZZI *et al.* (1987). Aerosol optical depth was estimated using relationships between surface visibility and aerosol optical depth given by Sturm (1981). Sun glint radiance L_g was estimated using sun-sensor geometry and surface wind speed data in a model by GUZZI *et al.* (1987).

After atmospheric effects have been removed, the remaining water leaving radiance is expressed as a subsurface reflectance according to ROBINSON (1985). The subsurface reflectance quantity can be regressed against *in situ* suspended sediment concentration (SSC) data; however, *in situ* data were not sufficient to establish reliable SSC regression coefficients for March 30 and April 1, 1989. Therefore, MAMS visible and near infrared reflectance images in this paper are displayed as a scaled subsurface reflectance quantity. Further discussion of the atmospheric correction of MAMS radiances can be found in GUMLEY *et al.* (1990).

Atmospheric Correction of Infrared Data

MAMS 11 μm and 12 μm infrared radiances were used to correct for atmospheric water vapor effects in estimating sea surface temperature (SST). A split window algorithm (MCMILLIN and CROSBY, 1984) was used

$$SST = T_{11} + A(T_{11} - T_{12}) + B$$

where T_{11} and T_{12} are the MAMS 11.2 μm and 12.5 μm brightness temperatures, A is a regression coefficient, and B is a bias correction. Robust values for A and B have not yet been determined for MAMS split window channels; because MAMS split window channels are similar to those of the geostationary VISSR Atmospheric Sounder (VAS), an instrument used previously to estimate SST (see BATES *et al.*, 1987), VAS SST coefficients were used. A bias correction between MAMS and VAS 11 μm and 12 μm radiances was applied to remove absolute calibration differences between the instruments. Tests using MAMS-specific SST coefficients under development showed only minor difference (<1 K) from using the VAS SST coefficients to estimate SST.

CASE STUDY RESULTS

Cold Front Passage of 31 March 1989

In the early spring of 1989, MAMS was deployed to Patrick AFB, Florida, for a series of flights along the Louisiana coast on NASA's ER-2 high altitude aircraft. The objective was to obtain MAMS imagery of coastal conditions during both pre-frontal and post-frontal phases of a cold front passage. This objective is difficult as pre-frontal mid and upper level clouds often obscure the coastline during the cold front season. However, a weak relatively cloud-free synoptic low which had formed in Texas on March 29, strengthened and proceeded with minimal cloudiness through the Louisiana coastal region with frontal passage occurring late on March 30 into early morning of March 31. MAMS was flown on the morning of March 30 twelve hours prior to frontal passage, and on the morning of April 1, about thirty-six hours after frontal passage.

The cold front propagated west to east at a high angle to that of the coastline orientation. Surface conditions created by this system are illustrated in a time series format in Figure 3 from observations made at the National Weather Service (NWS) station in Lake Charles (LCH), Louisiana. The frontal passage is well defined by the increase in surface pressure beginning about 0200 UTC on March 31 (8 pm LST, March 30). Decrease of air temperature behind the front is illustrated by the temperature minima on the days following the frontal passage (about 3–6 K). Dew point temperatures also decrease behind the front. Surface winds show maximum speeds in the 12 hours preceding and just after the frontal passage with a southwest to northerly wind shift. Thus, while MAMS flew in both the pre-frontal and post-frontal phases, it did not overfly the Louisiana coast during peak winds in either phase. Results of the wind forcing during those peak velocity periods

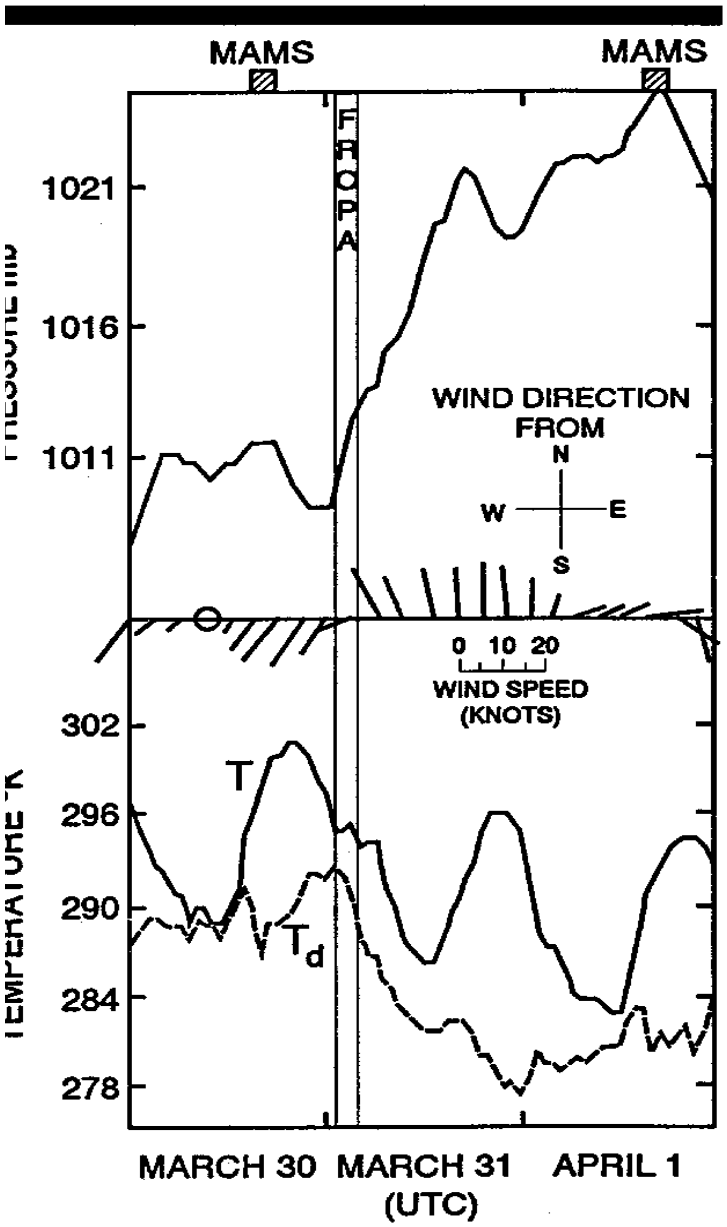

Figure 3. Surface observations of pressure, wind, temperature (T) and dew point (T_d) at Lake Charles (LCH), Louisiana, from March 30 through April 1, 1989. A cold front passage at Lake Charles is indicated by FROPA. MAMS data collection periods are indicated by blocks at top of diagram.

however are seen in the imagery because hours are required to establish the wind driven coastal and estuarine circulation.

The wind forcing by a cold front may be quantitatively evaluated by a summation of the wind energy over time as a function of wind direction. A simple kinetic energy approach is to square the wind speed and compute the component over the spectrum of wind directions. This summation is plotted as a function of wind direction in the top of Figure 4 for the NWS station at Lake Charles (LCH), Louisiana, located about 40 km inland. Energy curves are plotted for 24 hour summation periods beginning on March 30. Note that surface wind speeds are likely to be significantly greater over the open nearshore waters than over land (Hsu, 1981). Maximums in the southwesterly (pre-frontal; March 30) and northerly (post-frontal day 1; March 31) directions are obvious and represent the strongest portions of the pre-frontal and post-frontal phase winds respectively. Wind conditions during the MAMS flight on April 1 (post-frontal day 2) were weaker and more easterly (becoming more southeasterly later in the day, signalling the transition into the next pre-frontal phase; see Figure 3). The observed coastal temperature and turbidity patterns on April 1 therefore depict coastal waters under a weaker forcing than existed at earlier times in the cold front cycle. Data collection during peak periods of wind forcing is desirable to fully understand the impact during the cold front cycle. The absolute magnitude of the cold front wind energy is best understood in comparison to that of other cold front passages. In the bottom of Figure 4, overlain on the March/April 1989 data, is the wind energy spectrum for a strong north to south propagating cold front that passed through LCH on December 22, 1990. The December 1990 energy in the pre-frontal phase is more than twice that of the March/April 1989 case. Energy in the 24 hours following cold front passage (post-frontal day 1) is similar for each case, however post-frontal day 2 energy for the December 1990 case far exceeds that of the March/April 1989 case. This comparison shows that the March 1989 case involved only a modest level of wind energy. There is a need to collect data on more cold front passage cases so that understanding can be advanced on how factors such as cold front strength, speed of propagation,

→

Figure 4. Cumulative surface wind energy for 24 hour periods of pre-frontal, post-frontal day 1, and post-frontal day 2 as a function of wind direction for observations at Lake Charles, Louisiana, on March 30–April 1, 1989 (top and bottom), and December 21–23, 1990 (bottom). Wind energy, primarily southerly in pre-frontal conditions (solid lines), shifts to northerly directions after frontal passage (dashed lines). Note the scaling change in the bottom graph, which is presented as a comparison of the wind energy from a strong (December 21–23) and a modest (March 30–April 1) cold front case.

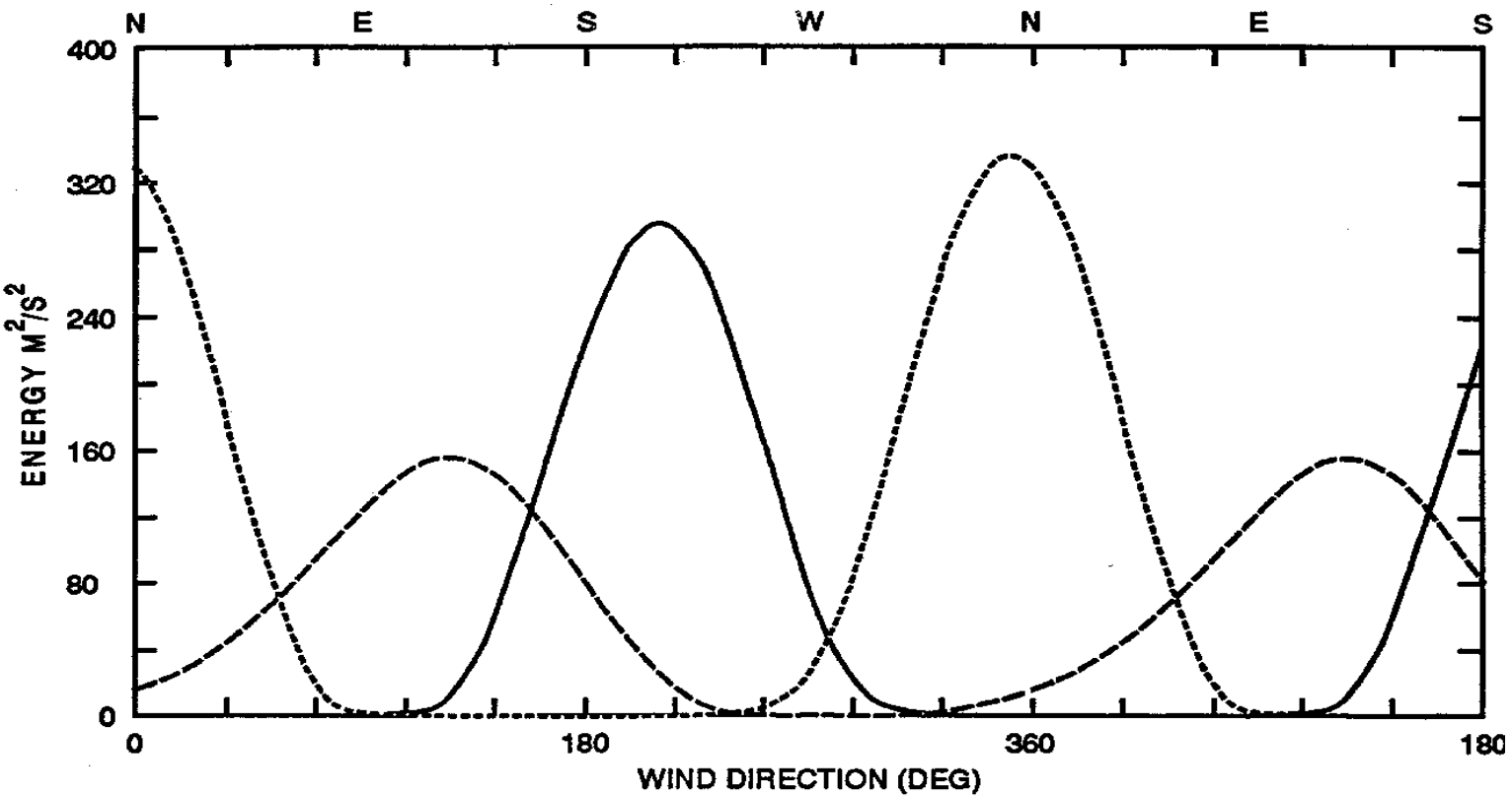

PREFRONTAL MARCH 30
POSTFRONTAL MARCH 31
POSTFRONTAL APRIL 1
PREFRONTAL DEC 21
POSTFRONTAL DEC 22
POSTFRONTAL DEC 23

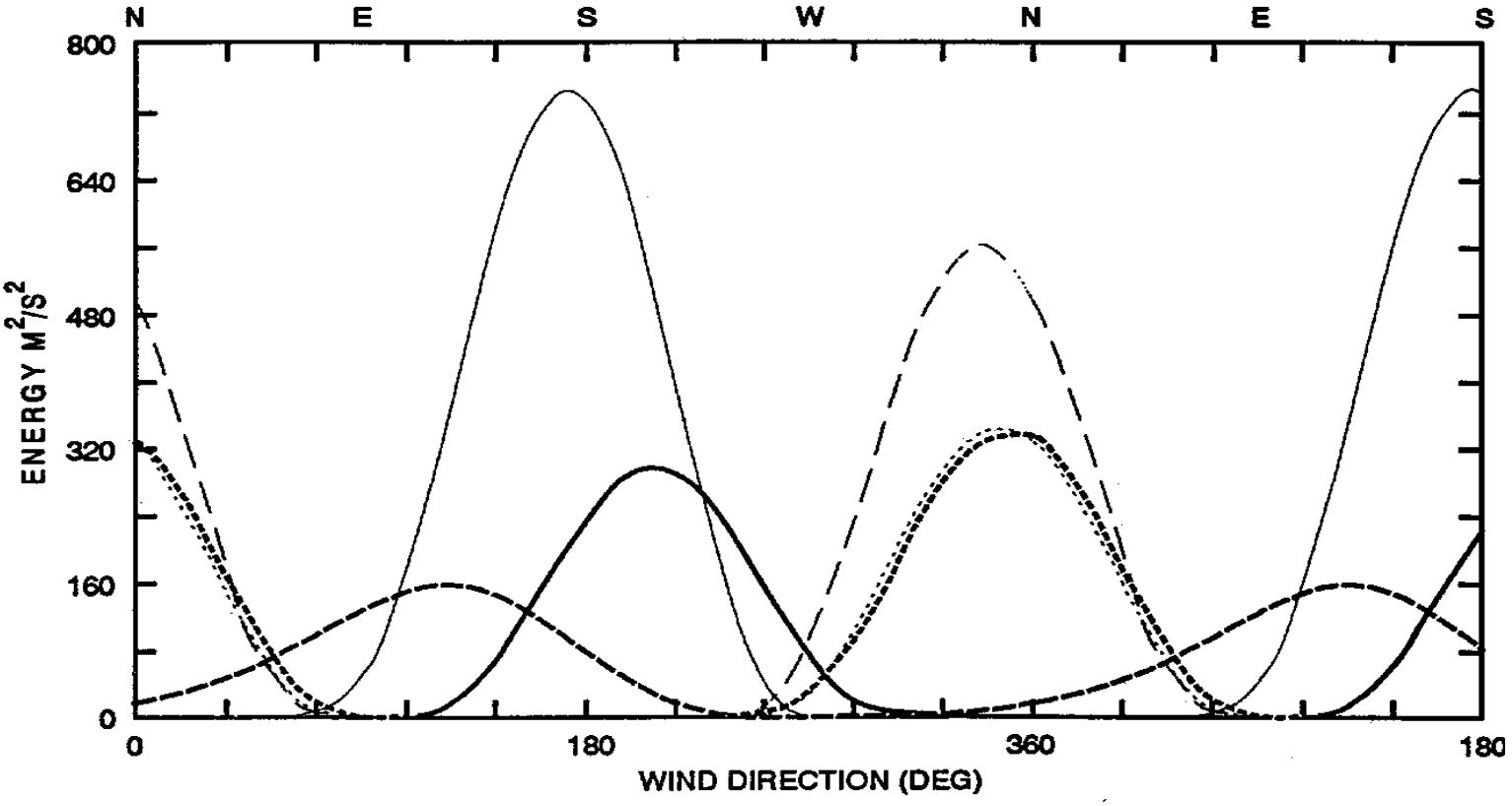

and angle of approach affect the response of the coastal environment. These factors affect the coastal wave and current generation in addition to sea level setup and setdown.

Response of Sediment Plumes

The sediment load of the Mississippi River is split between two distributaries, the Mississippi River delta and the Atchafalaya River delta. The Atchafalaya River (including the Red River flow) discharge is 30% of the volume and 50% of the suspended sediment load of that in the Mississippi River (MOSSA and ROBERTS, 1990). The Atchafalaya Bay sediment discharge plume is a primary source of depositional material for the western Louisiana coastal zone including the Chenier Plain region. Cold front passages create a "pulse" of increased Atchafalaya Bay discharge onto the continental shelf. Whether the sediments in the discharge plume are deposited directly onto the shoreface or onto the subaqueous bottom, coastal progradation relies on an influx of this material. Because of this, it is useful to determine the response of the Atchafalaya Bay sediment plume to cold front systems. The Atchafalaya Bay sediment plume is shown in Figure 5 for the MAMS flights on March 30 and April 1. Southwesterly winds on March 30 (top) retarded the westward flow of the plume (yellow/red in Figure 5) towards the Chenier Plain, creating a damming effect which forced the sediment plume southward out of the Atchafalaya Bay into the Gulf of Mexico (beyond the southern extent of the MAMS imagery). This restricted the flow of depositional material towards the Chenier Plain. Under these conditions, only resuspended bottom sediments (by wave action) are available for deposition on the Chenier Plain shoreface. Otherwise, with low sediment content, wave action is an erosive force on the Chenier Plain coastline. On April 1 (bottom), with easterly winds, the plume extended westward along the Chenier Plain coast, transporting high levels of suspended sediment to that area. Very little of the plume extended southward on April 1. This is seemingly a direct response of the sediment plume to surface winds, exhibiting an important dependence of the coastal environment on cold front systems.

The main channel of the Mississippi River carries about 70% of the Mississippi River's sediment load to the Gulf of Mexico. The modern Mississippi birdfoot (Balize) subdelta, some 600–800 yr old, has prograded to near the edge of the continental shelf. Sediment carried to the Gulf is visible as narrow, linear plumes emanating from the various outlet points of the delta. The sediment is dispersed, gradually settling out of the plumes into relatively deep waters. Thus, little or no coastal progradation is taking place near the Mississippi River delta. The pattern of sediment plumes around the birdfoot delta are shown in Figure 6. Like the response in the Atchafalaya Bay region on March 30, sediment outflow appears to be blocked from the southwest, resulting in pooling of high turbidity water (green/yellow) on the southwest side of the delta. On April 1, northeasterly to easterly winds concentrate turbid water on the northeast side of the delta, while the turbid water on the southwest side appears to have largely dispersed. Plumes on the southwest side of the delta suggest that the turbid water has dispersed downwind.

Coastal Circulation Response

The rise and fall of water levels as well as the winds in coastal regions affects coastal circulation patterns. Astronomical tides cause water levels to rise and fall on a regular and predictable basis. Because the Louisiana coast is a microtidal coast (astronomical tides have a range of only about 0.5

→

igure 5 (top). MAMS images of subsurface reflectance in the Atchafalaya Delta/Chenier Plain area (refer to map in Figure 1) on larch 30 (top) and April 1 (bottom), 1989. North is towards the top of the page. Relatively clear water is purple/blue; highly turbid ater is yellow/red. Land is shaded white. The data is subsampled to 300 m resolution to display the entire flight track in the image. n March 30, southwesterly winds retard sediment flow towards the west, forcing the sediment plume out into the Gulf of Mexico o the south; on April 1, easterly winds force the plume westward along the coast, reducing its southward extent into the Gulf of lexico.

'igure 6 (bottom). MAMS subsurface reflectance at the Mississippi birdfoot delta (refer to map in Figure 1) on March 30 (left) nd April 1 (right). North is towards the top of the page. Land is shaded white. Relatively clear water is blue; turbid water is green o yellow. The data is subsampled to 200 m resolution. On March 30, southwest surface winds caused sediment to pool on the outhern and western sides of the delta. With northeast surface winds on April 1, sediment is concentrated on that side of the delta /hile sediment pools on the southwest side have largely dispersed.

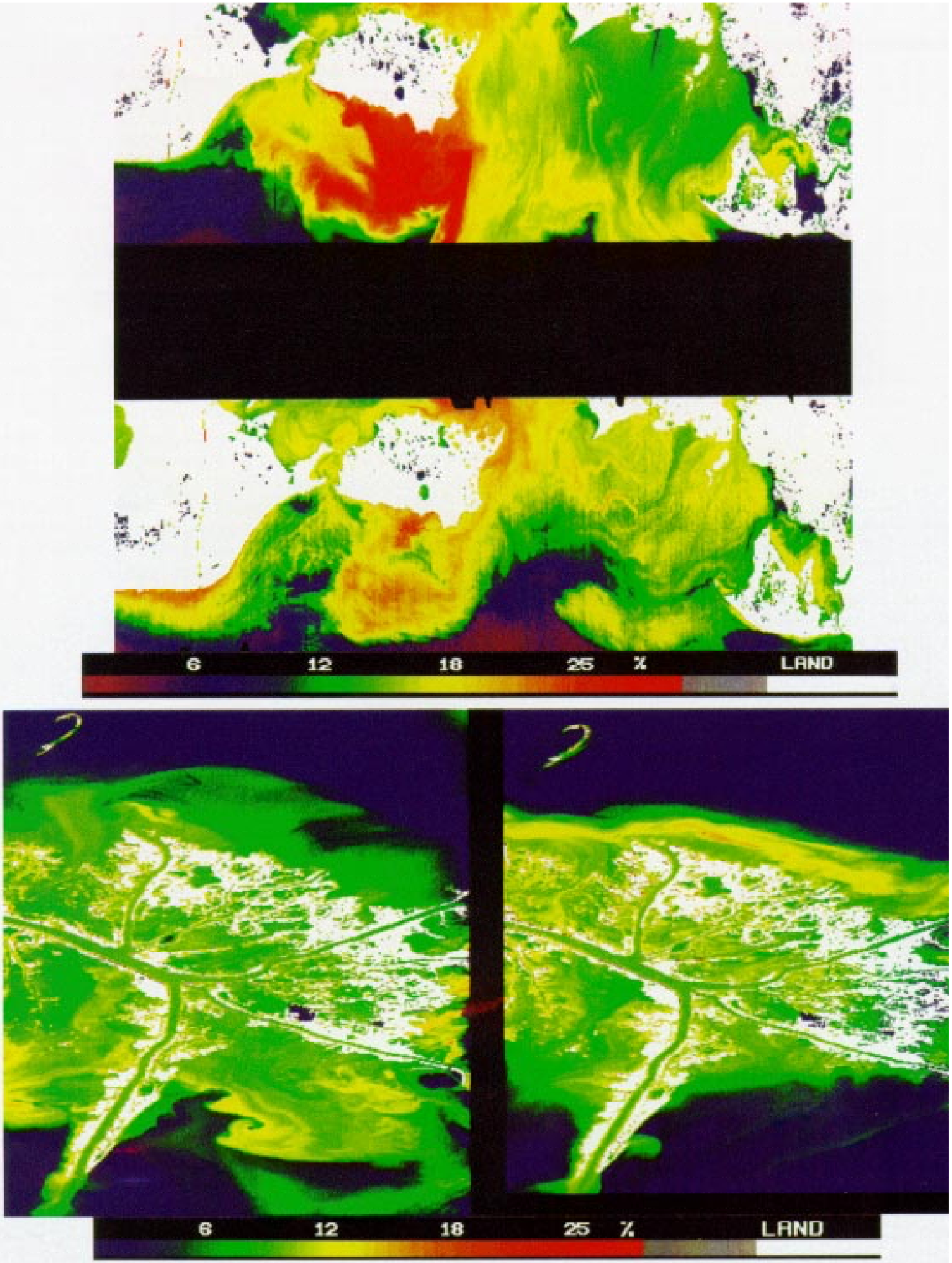
6
12
18
25
%
LAND
6
12
18
25
%
LAND

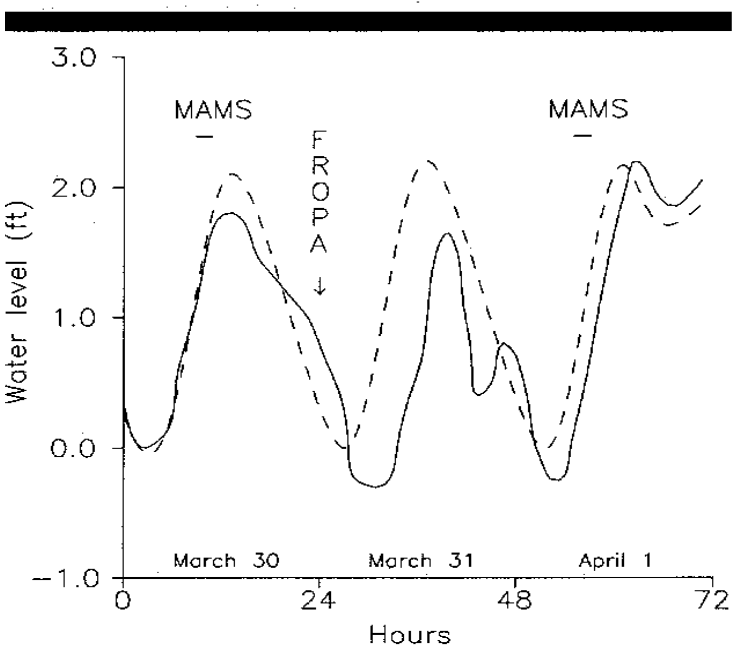

Figure 7. Predicted (dashed) and observed (solid) water levels at Eugene Island, Louisiana. Values are differences from their respective low water on the morning of March 30. Data plotted begins at midnight local time on March 30. Predicted tide data is taken from tables compiled by the U.S. Coast and Geodetic Survey. Observed water level data courtesy of U.S. Army Corps of Engineers, New Orleans District. MAMS data collection periods indicated by bars at top. Time of frontal passage at Eugene Island indicated by FROPA.

meters), winds of a cold front system induce relatively large, but lower frequency changes in water level. Onshore winds, the pre-frontal southerlies, and decreasing barometric pressure set up sealevel along the coast. This increases bay and estuary water levels, temporarily "damming up" the inflowing rivers. Offshore winds, the post-frontal northerlies, and rising barometric pressure set down coastal water levels, spilling river, marsh, bay and estuarine waters seaward onto the continental shelf. The actual water level is the result of the combined influence of astronomical tides and surface winds. The different but regular time scales of these two forces, (diurnal *vs.* 3–6 days) add to water level variability as they go in and out of phase. The response of water level to the cold front winds of March 30–April 1 can be seen in water level data collected at Eugene Island in the Atchafalaya Bay (Figure 7). Predicted astronomical tide data for Eugene Island is also shown. During southerly winds on March 30, water level closely follows the predicted tidal range until about midday (12 hours before the frontal passage) when water levels begin to drop more slowly than the predicted tides. After frontal passage during the night of March 30–31, winds become more northerly and water level drops quickly while tides are predicted to increase. A subdued high water level on March 31 follows, this all occurring under the strong northerly winds that followed the frontal passage (see Figure 3). Water level and predicted tides work back into agreement with each other when the northerly winds weaken on April 1. Interestingly, water level range exceeds predicted tide range when winds turn back out of the southeast later in the day on April 1. This is a case where wind and astronomical tide forcings were out of phase. Had they been in phase, the range of the observed water level plot probably would have doubled.

While it is difficult to discern the various scales of motion which are surely present in a "snapshot" of a coastal scene, some circulation patterns in the Atchafalaya Bay are identifiable in Figure 8. Figure 8 demonstrates small scale (<1 km) circulation changes affected by cold front passages. The SST imagery shows an arm of cold (dark) water (point A) flowing eastward from Atchafalaya Bay into Four League Bay on March 30. Thin, warmer (lighter) streamlines off the Atchafalaya delta (point B) also indicate flow towards Four League Bay. It is also somewhat apparent that cooler bay water extends south and east (point C) around Point Au Fer Island out of the bay. This pattern is also visible in the subsurface reflectances for March 30 in Figure 5. On April 1, with easterly winds, cold streamlines near the Atchafalaya delta (point B) appear to be draining southward towards the Gulf, bypassing Four League Bay. An arm of warmer marsh drainage water appears to be cutting between Atchafalaya Bay and the entrance to Four League Bay (point A). Evidence of this relatively clear marsh drainage also exists in the subsurface reflectance data (thin, blue streamline in Figure 5). Cold Atchafalaya Bay waters extend westward (point C) out of the Bay in agreement with the pattern shown for April 1 in Figure 5.

Circulation patterns in the Chandeleur Islands/birdfoot delta region are depicted using SST imagery in Figure 9. On March 30 an extended coastal zone of cold (dark) water exists on the northeast (lee) side of the delta. Water on the southwest (windward) side appears diffuse and shows little in the way of circulation patterns. On April 1, the coastal zone on the northeast (windward) side of the delta has a smaller seaward extent. On the

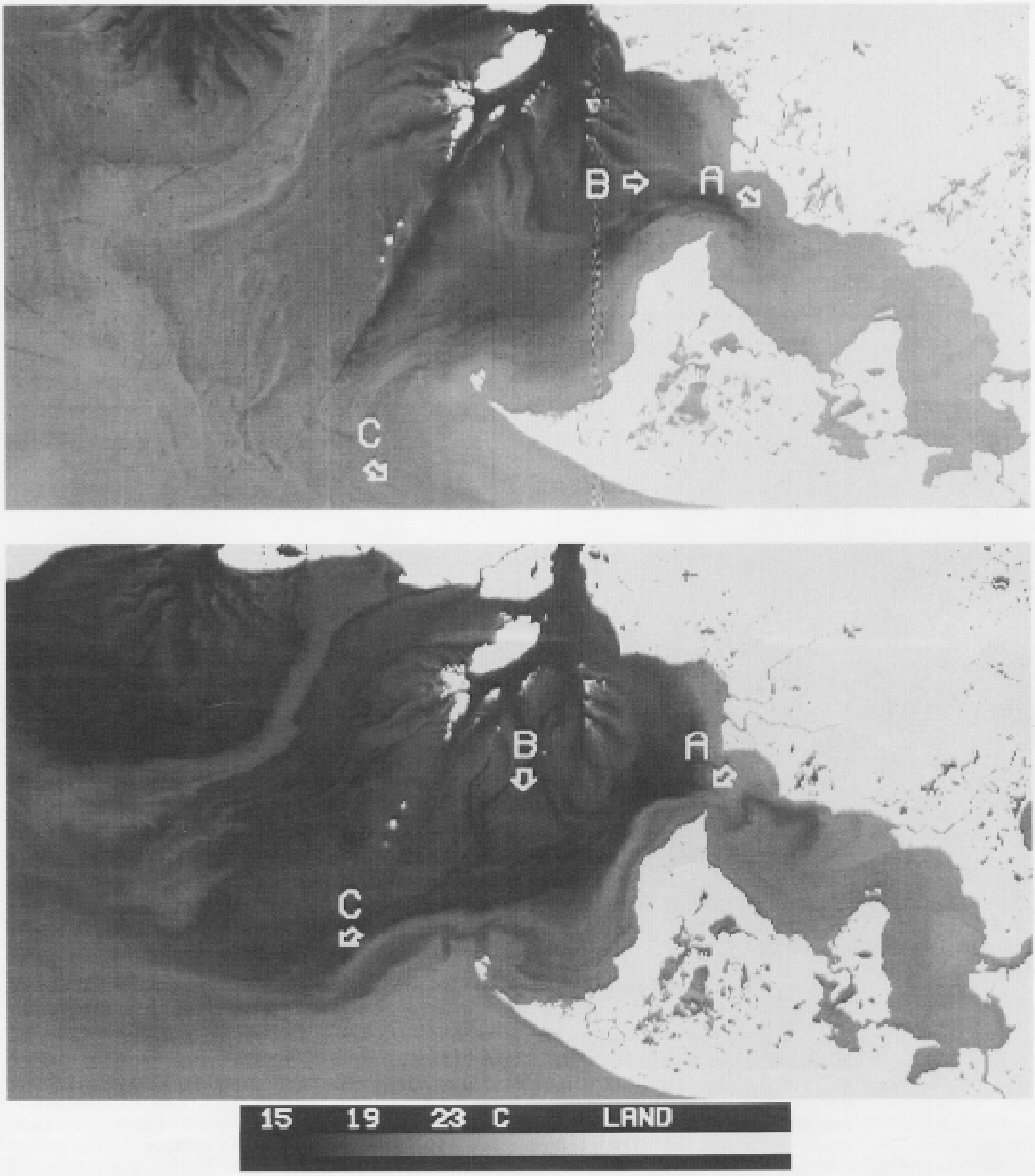

Figure 8. MAMS SST imagery in the Atchafalaya Delta area (refer to Figure 1 for map) on March 30 (top) and April 1 (bottom). Land is shaded white. Dark shades are cold. North is towards the top of the page. Thermal contrast shows evidence of flow in the water on each day. Arrows indicate direction of flow. See text for discussion.

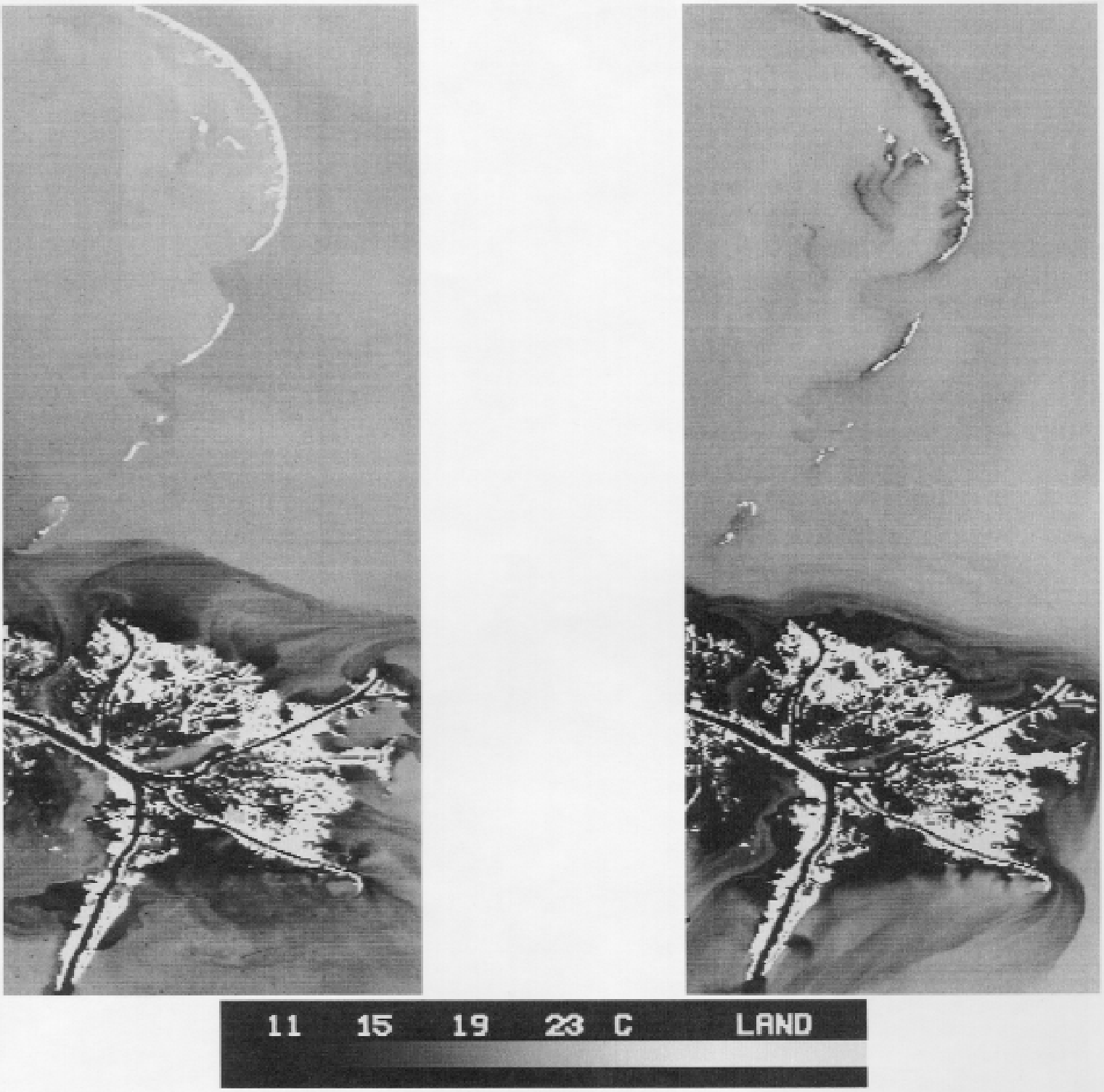

Figure 9. MAMS SST imagery in the Mississippi birdfoot delta/Chandeleur Islands area (refer to Figure 1 for map) on March 30 (left) and April 1 (right). North is towards the top of the page. Dark shades are cold. Land is shaded white. The data is subsampled to 300 m resolution. The coastal front around the birdfoot delta (bottom of each image) is indicated by a strong thermal gradient. On the northeast side of the delta, the coastal front extends much further out on March 30 than it does on April 1. Also note cooler SST's in the shallow waters on the western side of the Chandeleur Islands (top center of each image) on April 1 *vs.* March 30. Thermal contrast also shows evidence of flow in the water on each day.

southwest (lee) side of the delta, streamlines of cold water extend downwind towards the southwest. This suggests that circulation patterns around the birdfoot delta respond quickly (<24 hours) to surface wind conditions. This agrees with the response time indicated in the water level analysis of Figure 7. In the open water region surrounding the Chandeleur Islands it is difficult to discern circulation patterns on March 30. Weak westward intrusions of cool water between the islands into backbay waters are visible. Circulation in backbay waters west of the islands is difficult to identify. By contrast on April 1, cool water streamlines from small backbay islands indicate a southward drift. Northeast to east winds on April 1 probably contribute to this drift. The westward extent of the intrusions between the islands is also increased suggesting a stronger entrainment of water into the backbay region. These intrusions may accelerate the transport of sandy deposits between the barrier islands into the backbay region.

The circulation analysis would benefit greatly by animating MAMS repeated overpass scenes. Unfortunately, due to the myraid of aircraft motions, it is currently very difficult to geometrically rectify MAMS data accurately enough to animate multiple scenes. Research to improve image rectification (for MAMS and other airborne sensors) to the single pixel accuracy that is presently possible with geostationary satellite data is in progress (RICKMAN *et al.*, 1989). This would allow animation of the fine scale (0.1–5 km) water motions that exist in these dynamic coastal environments.

SST Response to Atmospheric Conditions

Change of SST with time is dependent on several fluxes, namely the terms of the heat exchange equation: solar flux, sensible and latent heat flux, radiative heat flux, and advection of heat in the water column. For carefully chosen locations, solar flux (clear skies both days) and, with somewhat more uncertainty, advection of heat can be assumed to be approximately constant on March 30 and April 1. This leaves sensible, latent, and radiative heat fluxes, which all vary as a function of atmospheric conditions, as responsible for most of the SST change from March 30 to April 1. Strictly speaking, SST represents the temperature of the water's skin, not the entire water column as is specified in the heat exchange equation. However, if the water column is well mixed, as in the windy conditions of cold front passages, then changes in SST become representative of changes in the entire water column. Knowing that the heat content of the water column is a function of water depth and assuming equal fluxes over a spatial domain, shallow water columns should heat and cool the most rapidly as atmospheric conditions change. This idea was examined in the MAMS SST data for March 30 and April 1.

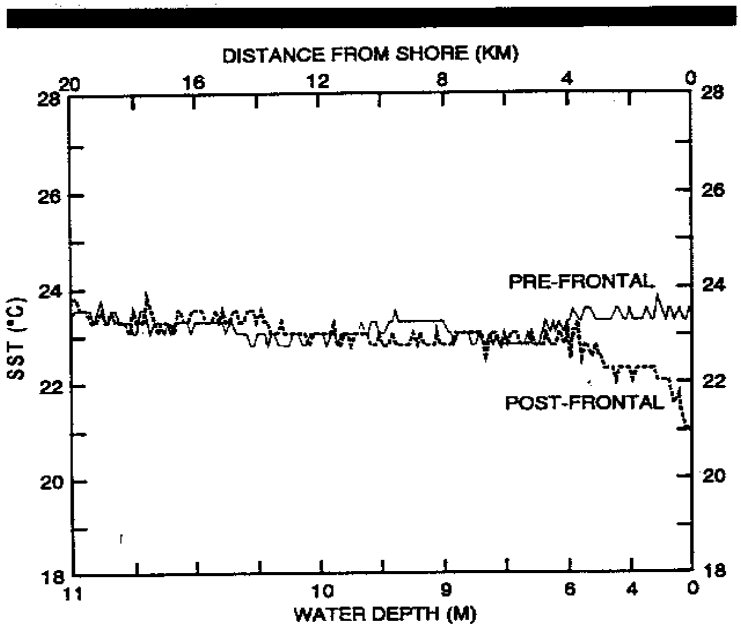

Figure 10. MAMS SST transects along the Chenier Plain coast for pre-frontal phase on March 30 (solid) and post-frontal phase on April 1 (dashed). SST increases towards shore in the warm pre-frontal conditions of March 30, and decreases towards shore in the colder post-frontal conditions on April 1.

Figure 10 shows a MAMS SST transect extending from the Chenier Plain coast outward into the progressively deeper waters of the Gulf of Mexico on March 30 and April 1. The location was chosen to minimize ambiguities resulting from advection of different water types through the transect. As was indicated in Figure 3, air temperature dropped some 3 to 6 K over this period with a corresponding drop in dew point temperature. SST response to the atmospheric variation is related to water depth in Figure 10. Little response is apparent in waters deeper than about 6 meters. As water depth decreases towards the shore, the response increases. A maximum cooling of about 2.5 K occurs within a few hundred meters of shore. This quick response to changing atmospheric conditions is a result of the lower heat content of shallow waters. In deeper waters, ver-

tical mixing and larger stored heat content maintain the SST at a nearly constant temperature. A similar response can be seen in Figure 9 around the Chandeleur Islands. Near the islands, water temperatures are significantly cooler on April 1 than on March 30. Deeper waters show little change. Decreases of about 2–3 K from March 30 to April 1 have also been seen in MAMS SST data in the shallow Barataria Bay region of the Louisiana coast as well as in inland lakes.

CONCLUSIONS

MAMS has been used to study the response of Louisiana coastal waters to atmospheric forcings associated with individual cold front passages. Linking atmospheric forcings to dynamic responses in the coastal environment is an important approach for understanding processes of coastal change. One hundred meter resolution images collected during the pre-frontal and post-frontal phases of a March, 1989 cold front event are among the first high resolution images known to the authors to document the coastal response to a cold front. The wind, pressure, temperature, and humidity characteristics of the cold front passage force changes in the coastal environment. Atmospherically corrected visible and near infrared imagery show that sediment flowing out of the Atchafalaya Bay is deflected downwind by post-frontal winds, displacing the source of depositional material for coastal progradation. Coastal circulation patterns vary in response to wind, water level, and river discharge, all forced or modulated by cold front winds. SST imagery provides information on timing and extent of the temperature response of shallow coastal regions to atmospheric conditions. These are reliable in the absence of significant thermal advection and horizontal mixing of water types.

Coastal waters evolve continuously during the cold front event. The MAMS data shown in this paper provide a discrete look at the continuous responses to a single cold front event. Coastal circulation, plume dispersal, and sea surface temperature patterns during peak forcing conditions on March 31 would likely have revealed even stronger responses to the winds during the post-frontal phase of the cold front (as is indicated in Figure 7 by the response of water level to the winds just after frontal passage) had the MAMS instrument been flown on that day. Also of interest is the response of coastal waters and sediments to cold fronts of varying intensity, propagation speed, and angle of approach. Further, the question of cumulative impact over a winter season, especially as compared to the impact of tropical storms and hurricanes, has received very little attention. Preliminary work (Huh *et al.*, 1978) suggests that coastal and continental shelf waters evolve continuously in response to the seasonal succession of cold front passages, with chilled shelf waters spreading progressively seaward from inshore to shelf edge.

ACKNOWLEDGEMENTS

The authors gratefully acknowledge NASA funding under Grants NAGW-2052, to Louisiana State University, from Geology Programs, under Dr. Miriam Baltuck for surface truth, and NAGW-1745 to the University of Wisconsin, from Atmospheric Programs, under Dr. James Dodge for MAMS ER-2 data collection and analysis. Special appreciation is extended to the NASA Ames Research Center's High Altitude Missions Branch; without their tireless efforts, it would not have been possible to collect the excellent MAMS data set used in this paper.

LITERATURE CITED

Bates, J.J.; Smith, W.L.; Wade, G.S., and Woolf, H.M., 1987. An interactive method for processing and display of sea-surface temperature fields using VAS multispectral data. *Bulletin of the American Meteorological Society,* 68, 602–606.

Gordon, H.R.; Clark, D.K.; Brown, J.W.; Brown, O.B.; Evans, R.H., and Broenkow, W.W., 1983. Phytoplankton pigment concentrations in the Middle Atlantic Bight: Comparison of ship determinations and CZCS estimates. *Applied Optics,* 22, 20–36.

Gordon, H.R., 1978. Removal of atmospheric effects from satellite imagery of the oceans. *Applied Optics,* 17, 1631–1636.

Gumley, L.E.; Moeller, C.C., and Menzel, W.P., 1990. Monitoring of Mississippi delta coastal geomorphology using high resolution Multispectral Atmospheric Mapping Sensor (MAMS) data. *5th Australasian Remote Sensing Conference* (Perth, Australia), pp. 738–745.

Guzzi, R.; Rizzi, R., and Zibordi, G., 1987. Atmospheric correction of data measured by a flying platform over the sea: Elements of a model and its experimental validation. *Applied Optics,* 26, 3043–3051.

Hsu, S.A., 1981. Models for estimating offshore winds from onshore meteorological measurements. *Boundary Layer Meteorology,* 20, 341–351.

Huh, O.K.; Wiseman, W.J., Jr., and Rouse, L.J., Jr., 1978. Winter cycle of sea surface thermal patterns, northeastern Gulf of Mexico. *Journal of Geophysical Research,* 83(C9), 4523–4529.

Huh, O.K.; Roberts, H.H., Rouse, L.J., and Rickman, D.A., 1991. Fine grain sediment transport and deposition in the Atchafalaya and Chenier Plain sedi-

mentary system. *Coastal Sediments '91: Proceedings of Specialty Conference* (June 25–27, 1991, Seattle, Washington), American Society of Civil Engineers, New York, pp. 817–830.

JEDLOVEC, G.J.; BATSON, K.B.; ATKINSON, R.J.; MOELLER, C.C.; MENZEL, W.P., and JAMES, M.W., 1989. Improved capabilities of the Multispectral Atmospheric Mapping Sensor (MAMS). NASA Technical Memorandum 100352, Marshall Space Flight Center, Huntsville, Alabama, 71pp.

KEMP, G.P., 1986. Mud Deposition at the Shoreface: Wave and Sediment Dynamics on the Chenier Plain of Louisiana. Ph.D. Dissertation, Louisiana State University, 146p.

MCMILLIN, L.M. and CROSBY, D.S., 1984. Theory and validation of the multiple window sea surface temperature technique. *Journal of Geophysical Research*, 89(C3), 3655–3661.

MOELLER, C.C.; GUMLEY, L.E., MENZEL, W.P., and STRABALA, K.I., 1989. High resolution depiction of SST and SSC from MAMS data. *Fourth Conference on Satellite Meteorology and Oceanography* (AMS, Boston, Massachusetts), pp. 208–212.

MOSSA, J. and ROBERTS, H.H., 1990. Synergism of riverine and winter storm related sediment transport processes in Louisiana coastal wetlands. *Transactions of the Gulf Coast Association of Geological Societies*, XL, 635–642.

RICKMAN, D.; OCHOA, M.C.; HOLLADAY, K.W., and HUH, O.K., 1989. Georeferencing airborne imagery over new deltas in Louisiana. *Photogrammetric Engineering and Remote Sensing*, 55, 1161–1165.

ROBERTS, H.H.; HUH, O.K.; HSU, S.A.; ROUSE, L.J., JR., and RICKMAN, D., 1987. Impact of cold-front passages on geomorphic evolution and sediment dynamics of the complex Louisiana coast. *Coastal Sediments '87, Proceedings of a Specialty Conference* (May 12–14, 1987, New Orleans, Louisiana). American Society of Civil Engineers, New York, pp. 1950–1963.

ROBINSON, I.S., 1985. *Satellite oceanography—An introduction for oceanographers and remote-sensing scientists.* Chichester, United Kingdom: Ellis Horwood, 150p.

STURM, B., 1981. The atmospheric correction of remotely sensed data and the quantitative determination of suspended matter in marine water surface layers. *In:* CRACKNELL, A.P. (ed.), *Remote Sensing in Meteorology, Oceanography, and Hydrology*. Chichester, United Kingdom: Ellis Horwood, pp. 163–197.